Neurobiology of Disease 86 (2016) 75–85

Contents lists available at ScienceDirect

Neurobiology of Disease

journal homepage: www.elsevier.com/locate/ynbdi

A mutation in the Warburg syndrome gene, *RAB3GAP1*, causes a similar syndrome with polyneuropathy and neuronal vacuolation in Black Russian Terrier dogs

Tendai Mhlanga-Mutangadura [a], Gary S. Johnson [a], Robert D. Schnabel [b,c], Jeremy F. Taylor [b], Gayle C. Johnson [a], Martin L. Katz [d], G. Diane Shelton [e], Teresa E. Lever [f], Elizabeth Giuliano [g], Nicolas Granger [h], Jeremy Shomper [g], Dennis P. O'Brien [g,*]

[a] Department of Veterinary Pathobiology, University of Missouri, Columbia, USA
[b] Division of Animal Sciences, University of Missouri, Columbia, USA
[c] Informatics Institute, University of Missouri, Columbia, USA
[d] Mason Eye Institute, University of Missouri, Columbia, USA
[e] Department of Pathology, University of California, San Diego, La Jolla, USA
[f] Department of Otolaryngology, University of Missouri, Columbia, USA
[g] Department of Veterinary Medicine & Surgery, University of Missouri, Columbia, USA
[h] School of Veterinary Sciences, University of Bristol, Langford House, Langford, Somerset BS40 5DU, UK

ARTICLE INFO

Article history:
Received 13 June 2015
Revised 13 November 2015
Accepted 18 November 2015
Available online 25 November 2015

Keywords:
Warburg micro syndrome
Martsolf syndrome
Spongiform encephalopathy
Endoplasmic reticulum
Rab GTPase
Membrane trafficking
Canine

ABSTRACT

An autosomal recessive disease of Black Russian Terriers was previously described as a juvenile-onset, laryngeal paralysis and polyneuropathy similar to Charcot Marie Tooth disease in humans. We found that in addition to an axonal neuropathy, affected dogs exhibit microphthalmia, cataracts, and miotic pupils. On histopathology, affected dogs exhibit a spongiform encephalopathy characterized by accumulations of abnormal, membrane-bound vacuoles of various sizes in neuronal cell bodies, axons and adrenal cells. DNA from an individual dog with this polyneuropathy with ocular abnormalities and neuronal vacuolation (POANV) was used to generate a whole genome sequence which contained a homozygous *RAB3GAP1*:*c.743delC* mutation that was absent from 73 control canine whole genome sequences. An additional 12 Black Russian Terriers with POANV were *RAB3GAP1*:*c.743delC* homozygotes. DNA samples from 249 Black Russian Terriers with no known signs of POANV were either heterozygotes or homozygous for the reference allele. Mutations in human *RAB3GAP1* cause Warburg micro syndrome (WARBM), a severe developmental disorder characterized by abnormalities of the eye, genitals and nervous system including a predominantly axonal peripheral neuropathy. *RAB3GAP1* encodes the catalytic subunit of a GTPase activator protein and guanine exchange factor for Rab3 and Rab18 respectively. Rab proteins are involved in membrane trafficking in the endoplasmic reticulum, axonal transport, autophagy and synaptic transmission. The neuronal vacuolation and membranous inclusions and vacuoles in axons seen in this canine disorder likely reflect alterations of these processes. Thus, this canine disease could serve as a model for WARBM and provide insight into its pathogenesis and treatment.

1. Introduction

Hereditary peripheral neuropathies, similar to human Charcot–Marie–Tooth disease (CMT), have been described in a number of dog breeds (Granger, 2011). As in CMT, the phenotypes in dogs are very heterogeneous ranging from predominantly demyelinating forms characterized by very slow motor nerve conduction velocities (MNCV) and histopathological evidence of demyelination, to predominantly axonal forms characterized by mildly slowed MNCV and axonal abnormalities on histopathology with many intermediate forms also recognized (Granger, 2011; Rossor et al., 2013; Vallat et al., 2013).

A predominantly axonal polyneuropathy is also reported as part of the Warburg micro syndrome (WARBM), a developmental disorder in humans affecting the eye, the nervous system and the genitals (Handley et al., 2013; Nassogne et al., 2000; Warburg et al., 1993). WARBM is caused by mutations in several genes that affect function of Rab GTPases (Aligianis et al., 2005; Aligianis et al., 2006; Bem et al., 2011; Liegel et al., 2013). The Rab GTPases regulate the formation and intracellular trafficking of membranous structures including endoplasmic reticulum (ER), endosomes, autophagosomes, and synaptic vesicles

* Corresponding author.
E-mail address: obriend@missouri.edu (D.P. O'Brien).
Available online on ScienceDirect (www.sciencedirect.com).

http://dx.doi.org/10.1016/j.nbd.2015.11.016

as well as formation of lipid droplets (Fischer von Mollard et al., 1990; Gerondopoulos et al., 2014; Hutagalung and Novick, 2011; Martin et al., 2005; Ozeki et al., 2005; Spang et al., 2014; Zirin et al., 2015).

A juvenile-onset laryngeal paralysis and polyneuropathy was reported in two Black Russian Terriers (BRT) (Granger, 2011). The dogs presented for respiratory distress due to laryngeal paralysis but also displayed ataxia, distal weakness, and reduced spinal reflexes. MNCVs and biopsies suggested an axonal disease (Granger, 2011). In the present study, we examined additional BRT and found that the disease phenotype includes polyneuropathy with ocular abnormalities and neuronal vacuolation (POANV). The objective of this study was to characterize the clinical and pathological phenotypes and to identify the mutation responsible for the disease.

2. Materials and methods

All studies were conducted with the approval of the University of Missouri, Animal Care and Use Committee and with the informed consent of the dogs' owners. Three, 3-month-old BRT (1 male, 2 females) with laryngeal paralysis and weakness were examined at the University of Missouri, College of Veterinary Medicine. Electrodiagnostic testing was performed under general anesthesia as previously described (Walker et al., 1979). Electromyography (EMG) was performed on laryngeal, appendicular, and epaxial muscles of all 3 dogs and tibial MNCV were determined on 2 dogs. Medical records were reviewed on 13 additional affected dogs including the 2 previously reported cases (Granger, 2011). Two dogs had fluoroscopic swallow studies. At the owners' request, the 3 dogs evaluated at the University of Missouri were euthanized by barbiturate overdose due to poor quality of life. Necropsies were performed on them and 4 additional cases. Left and right laryngeal nerves and muscles were collected for histopathology from 2 additional affected dogs. All tissues from affected dogs for histopathology were collected from dogs euthanized at 3 months of age. Control laryngeal muscles and nerves were collected from a 3 month old Standard Poodle euthanized due to another disease. Tissues were fixed in 10% buffered formalin prior to being embedded in paraffin. Five μm thick sections were stained with hematoxylin and eosin (H&E) (Bancroft and Gamble, 2008). Additional stains were oil red O to detect lipid, Luxol-fast blue/PAS for myelin (Sheehan and Hrapchak, 1980) and calbindin immunohistochemical staining for Purkinje cells (Henkel et al., 2005). All immunohistochemical stains were run with a positive control tissue and using an irrelevant antibody to detect non-specific staining.

Slices of the cerebellum obtained at necropsy immediately after euthanasia from 2 dogs were placed in 2.5% glutaraldehyde, 100 mM sodium cacodylate, pH 7.4 and incubated in this solution at room temperature until further processing. Control slices of cerebellum were collected and fixed in a similar fashion from a 1 year old normal Beagle euthanized for other reasons. Areas of the samples containing the roof nuclei and the cortex were post-fixed in osmium tetroxide and embedded in epoxy resin. Sections of the embedded tissues were cut at a thickness of 0.4 μm, mounted on glass slides, stained with toluidine blue and examined with light microscopy. Areas of interest were identified in these sections and the blocks from which they were cut were trimmed to include only these areas. Sections were cut from the trimmed blocks at thicknesses of 70 to 90 nm and mounted on copper electron microscopy grids. The sections were stained with lead citrate and uranyl acetate and were then examined and photographed using a JEOL JEM-1400 electron microscope equipped with a Gatan digital camera.

Unfixed muscle specimens were shipped overnight by a courier service under refrigeration to the Comparative Neuromuscular Laboratory at the University of California San Diego. Upon receipt, muscles were snap frozen in isopentane pre-cooled in liquid nitrogen and stored at −80 °C until further processed by a standard panel of histochemical stains and reactions (Dubowitz and Sewry, 2013). Immunohistochemical staining of muscle cryosections was performed using rabbit polyclonal antibodies against LC3 N terminal (1:100, Abgent AP1802a, Abgent, San Diego, CA, USA) and ubiquitin (1:250, Dako 2015-02, Dako Denmark A/S, Glostrup, Denmark) as markers for autophagy. Details of further processing are as previously described (Beggs et al., 2010). Additional muscle specimens were immersion fixed in 10% buffered formalin and embedded in paraffin. Peripheral nerve specimens were similarly fixed in 10% buffered formalin and then transferred into 2.5% glutaraldehyde upon receipt by the laboratory. Nerves were post-fixed in 1% aqueous osmium tetroxide for 3–4 h and then

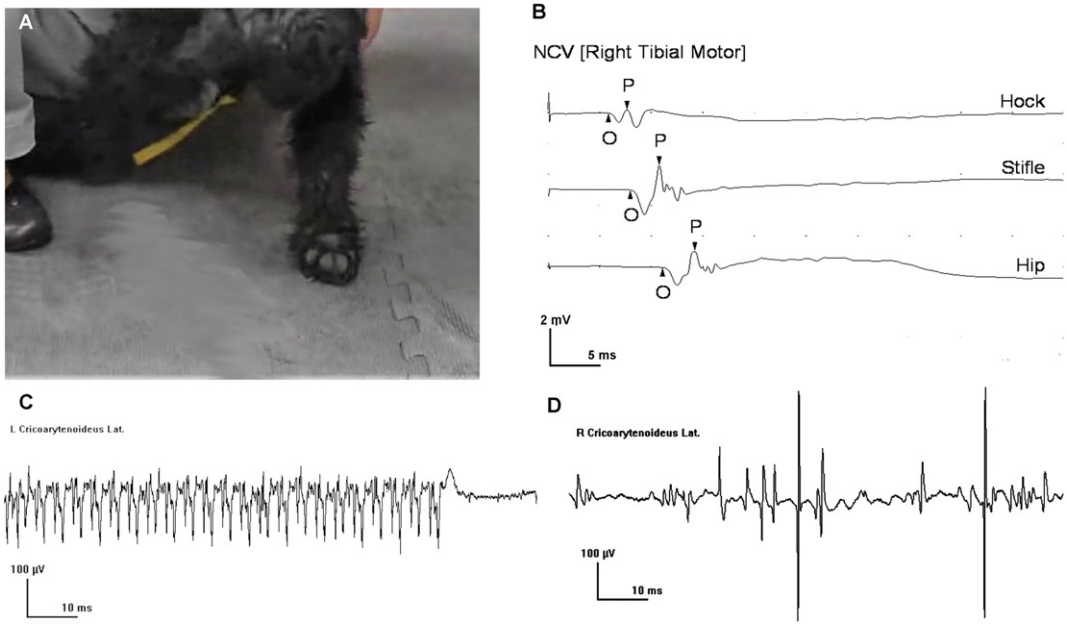

Fig. 1. Black Russian Terrier with POANV showing signs of sensory and motor polyneuropathy. A) Proprioception loss leads to failure to replace the paw when placed on the dorsum. B) Tibial motor nerve conduction showing decreased amplitudes (P = peak amplitude) and mild temporal dispersion suggesting axonal loss with only moderate slowing of conduction (O = onset of response). (C & D) EMG from cricoarytenoideus lateralis muscle showing complex repetitive discharge with an abrupt offset on the left side (C), and spontaneous fibrillation potentials on the right side (D) indicative of bilateral denervation..

dehydrated in graded alcohol series and propylene oxide. After infiltration with a 1:1 mixture of propylene oxide and araldite resin for 4 h, nerves were placed in 100% araldite resin overnight and then embedded in fresh araldite resin. Thick sections (1 μm) were cut with glass knives and stained with paraphenylenediamine prior to light microscopic examination. Thin sections (60–90 nm) were cut with glass knives and stained with uranyl acetate and lead citrate before examination with a Zeiss 10 electron microscope operating at 60 keV.

In addition to those collected from affected dogs and unaffected family members, DNA samples archived at the University of Missouri Animal Genetics Laboratory were used in this study. In all, we used DNA from the 262 BRT in our collection and samples from 100 randomly selected dogs representing 93 other breeds. Previously described methods were used to isolate DNA from EDTA-anticoagulated blood samples or from buccal swab samples on Whatman FTA® Elute cards (Katz et al., 2005; Zeng et al., 2014).

The libraries for generating a whole genome sequence (WGS) were prepared by Global Biologics (Columbia, MO) with DNA from a single POANV-affected BRT. The DNA sample was quantitated using the Qubit™ dsDNA HS Assay Kit and a Qubit® 2.0 Fluorometer (Life Technologies Inc.) and the DNA integrity was verified using a Fragment Analyzer (Advanced Analytical Tech Inc., Ames, IA). The DNA was sheared separately to ~300 bp and ~400 bp fragments with a QSonica plate sonication system (Qsonica Inc., Newtown, CT). The fragmented DNA was blunt end repaired, 3′ adenylated and ligated with multiplex compatible adapters using the Illumina NEXTflex DNA Sequencing Kit and size selected for ~300 bp and ~400 bp fragments with SPRI beads (Agencourt Inc.). PCR was used to amplify only those fragments with adapters on both ends. Size distributions for the resulting ~300 bp and ~400 bp libraries were verified with a Fragment Analyzer and libraries were quantitated by qPCR with the KAPA Library Quantification Kit (Kapa Biosystems Inc., Wilmington, MA).

The two libraries were sequenced at the University of Missouri DNA Core Facility with 2 × 100 paired-end runs on an Illumina HiSeq 2000 sequencer. Each library was sequenced in a separate flow cell lane. The sequence reads were deposited in the Sequence Read Archives (accession number SRS833812). Exact duplicate sequence read pairs were eliminated with NextGENe v2.3.2 software (SoftGenetics LLC, State College, PA) and adapter sequences were trimmed using custom Perl scripts. Unique adapter-trimmed reads were error corrected using MaSuRCA v1.9.5 software (Zimin et al., 2013). Error corrected reads were aligned to the CanFam3.1 reference genome assembly and variants called using NextGENe software. Variant calls were further processed using custom Perl scripts to filter likely false positives and then the variant calls were uploaded to a custom PostgreSQL database which contained the variant calls for an additional 73 canid WGS. Using custom SQL scripts we identified variants that fit an autosomal recessive mode of inheritance such that the case is homozygous for an allele not observed (heterozygous or homozygous) in any of the 73 control canid WGS. This candidate variant list was further filtered to include only variants predicted to alter the amino acid sequence of the encoded polypeptides. The controls included WGS from wild canids (n = 3), healthy dogs (n = 5), or dogs with heritable diseases other than PONAV (n = 65). Thirty four of the control WGS were from our group and 40 were generated elsewhere, as indicated in the Acknowledgments.

PCR primers *5′-ATGGCTGAAACCTCATCTCG-3′* and *5′-ACTCGCAGTAAT AAATATGTCA-3′* were designed to span an apparent *RAB3GAP1* frameshift mutation and produce an amplicon for direct sequencing to determine if the apparent variant was truly present in the DNA from the POANV affected dog. A TaqMan allelic discrimination assay (Livak, 1999) was used to genotype individual dogs at the *RAB3GAP1* frameshift mutation. For this assay, the PCR primers were *5′-ACTTCAGGATTGGCAG CAGTATTTT-3′* and *5′-ACTTAAAACCCACTGTTAAATAATTTCAATTTCCA-3′* and the competing probes were *5′-VIC-ACCTGGAGCTGCTG-MBG-3′* (variant allele) and *5′-FAM-ACCTGGAGGCTGCTG-MBG-3′* (reference allele).

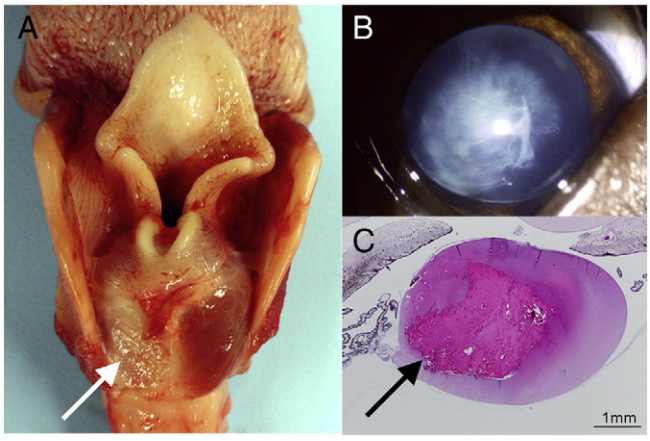

Fig. 2. Muscle atrophy and abnormal ocular development in POANV. (A) Larynx showing severe atrophy of the left cricoarytenoideus dorsalis muscle (arrow). (B) Late immature cataract seen on ocular examination. (C) Histopathological evidence of cataractous changes in the lens most notable in the nucleus (arrow).

3. Results

3.1. Clinical phenotype

Inspiratory stridor was noted in all affected dogs at 3 months of age, and sedated laryngeal examination identified bilateral laryngeal paralysis or left paralysis with right paresis. Of the 3 cases examined at the University of Missouri, one was in severe respiratory distress which prevented a thorough examination, while the other 2 exhibited normal behavior.

On ocular examination, bilateral abnormalities included microphthalmia (2 dogs), resting miotic pupils with incomplete dilation in dim light (3 dogs), late immature cataracts (3 dogs) (Fig. 2B), and iris to iris persistent pupillary membranes (2 dogs).

Sensory and motor deficits were observed in both neurological examination and fluoroscopic swallow studies. Sensory deficits included proprioceptive ataxia, postural reaction deficits (Fig. 1A), and pharyngeal retention of food. Motor deficits included pelvic limb weakness, hypotonia, diminished spinal reflexes, food bolus dyscohesion and delayed secondary peristalsis.

EMG showed prolonged insertional activity consistently in the laryngeal muscles and variably in the limb and epaxial muscles. In laryngeal muscles, spontaneous activity sometimes consisted of complex repetitive discharges with an abrupt ending (Fig. 1C). Spontaneous fibrillation potentials were also observed (Fig. 1D). Tibial MNCVs were moderately slow (41.9 and 35.9 m/s: reference range 53.0 ± 2.8 m/s (Swallow and Griffiths, 1977)). Compound motor unit action potential amplitudes were decreased (0.6 and 1.0 mV: reference range 13.8 ± 0.8 mV (Sims and Redding, 1980)) and showed mild temporal dispersion (Fig. 1B). All affected dogs died or were euthanized at the owners' request due to progressive weakness and/or respiratory distress by 6 months of age.

3.2. Molecular genetics

A 29.3 fold average coverage WGS was generated from the DNA of a single POANV-affected BRT and the sequence reads were aligned to the reference canine genome (build 3). From this alignment, we detected 71 homozygous sequence variants that were absent from the 73 control WGS and that were predicted to alter the amino acid sequence of the gene products. These variants occurred in 63 different genes and included 60 missense mutations, 8 frameshifts due to single nucleotide or dinucleotide insertions or deletions, 1 in-frame 3-nucleotide insertion, and 1 nonsense mutation (Supplementary Table 1). OMIM (http://

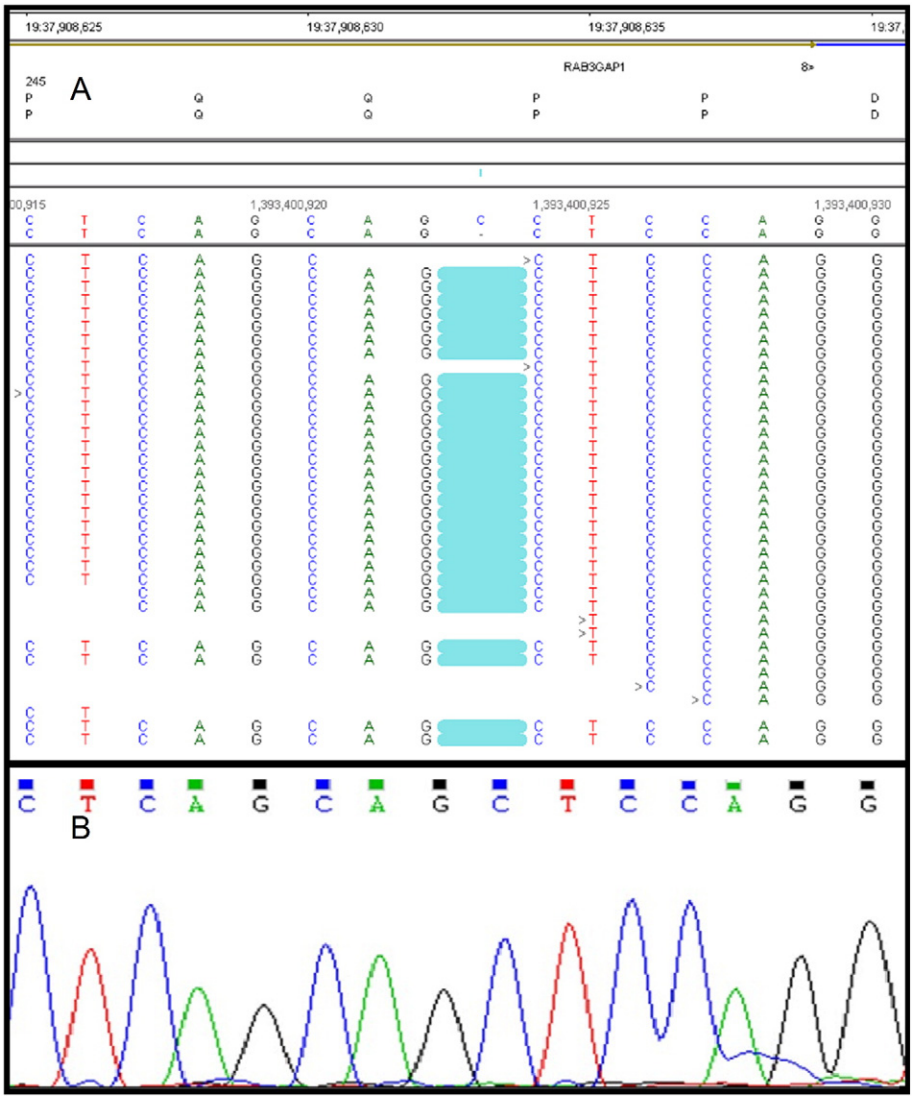

Fig. 3. Regional *RAB3GAP1* sequences generated with genomic DNA from POAVN-affected BRT. (A) Screen capture of NextGENe Viewer display of WGS sequence read alignment revealed the *RAB3GAP1*:*c.743delC* mutation; (B) automated Sanger sequencing verified the *RAB3GAP1*:*c.743delC* mutation.

www.ncbi.nlm.nih.gov/omim/) and PubMed (http://www.ncbi.nlm.nih.gov/pubmed) based literature reviews of the known functions and disease associations of the genes harboring these sequence variants suggested that *RAB3GAP1*:*c.743delC* (CanFam3.1 Chr19: 37,908,633) (Fig. 3A) was a plausible candidate for causing POANV because mutations in the human ortholog of this gene cause WARBM which is characterized by neurodevelopmental and ocular abnormalities in infants similar to those seen in the affected dogs. Direct automated Sanger sequencing confirmed that *RAB3GAP1*:*c.743delC* was an authentic homozygous sequence variant and not a sequencing artifact (Fig. 3B).

Archived DNA samples from all 262 BRT represented in our collection were genotyped at *RAB3GAP1*:*c.743delC*. In addition to the 3 POANV-affected BRT examined at the University of Missouri, 10 other samples were from dogs that exhibited clinical signs characteristic of POANV. This included a sample from one of the affected BRT described in a previous report (Granger, 2011). All 13 of these affected dogs were found to be homozygous for the *RAB3GAP1*:*c.743delC* variant. The other 249 genotyped BRT samples were either heterozygous at *RAB3GAP1*:*c.743delC* (n = 66) or were homozygous for the reference allele (n = 183). Among the 249 BRTs that were not *c.743delC* homozygotes, 223 were known to have survived past 6 months of age and, therefore, were unlikely to have POANV. We have limited clinical information for the remaining 26 BRTs that were not *c.743delC* homozygotes; however, 8 were reported by their owners to be normal when 4 months old or older and there were no indications in our records that any of the remaining 18 BRT have shown POANV-like clinical signs. Although the frequency of the *c.743delC* allele among the BRTs represented in our archived DNA samples was 0.18, this frequency is likely to be substantially higher than that for other BRT populations as many our samples were collected specifically because they were from dogs with POANV or their close relatives. The *c.743delC* allele was not detected in the DNA from 100 randomly selected purebred dogs of other breeds.

3.3. Macroscopic and histopathological phenotype

The most striking macroscopic necropsy findings were pallor and atrophy of laryngeal muscles, particularly the left cricoarytenoideus dorsalis muscle in all examined dogs (Fig. 2A). The eyes of two affected dogs were abnormally small and all three necropsied dogs exhibited bilateral cataracts at necropsy. Cataractous nuclear changes were noted on microscopic examination (Fig. 2C), with liquefaction and Morgagnian globules concentrated in this area.

No gross abnormalities were observed in the brain or spinal cord. Neuronal vacuolation was observed in the brain (4/4 dogs) and spinal cord (2/3 dogs). Vacuoles were abundant in the cerebellar roof nuclei (Fig. 4A) with 20% of the neurons having vacuoles (Supplementary

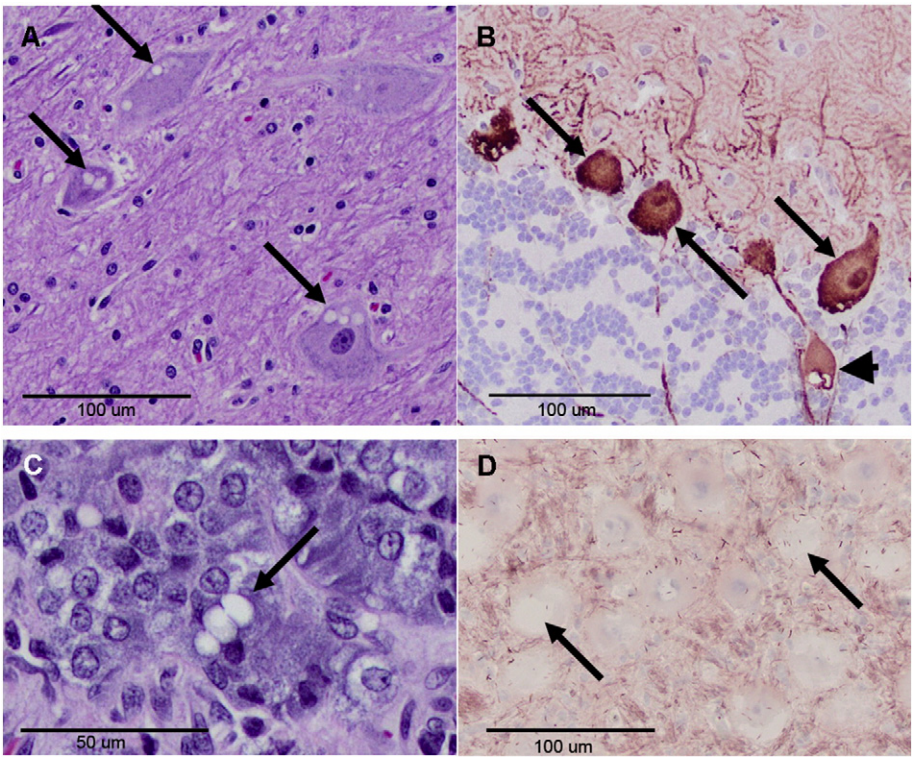

Fig. 4. Cytoplasmic vacuolation in dogs with POANV. (A) Many neurons in the cerebellar roof nuclei have cytoplasmic vacuoles (arrows) apparent on H&E stain. (B) Purkinje cells (arrows) show central pallor on calbindin staining with occasional enlarged axons with vacuolation (arrowhead). (C) Cytoplasmic vacuoles (arrow) in the adrenal medulla on H&E stain. (D) The neuronal vacuoles (arrows) in the cerebellar roof nuclei were negative with oil red O stain for lipids.

Table 2). Vacuoles could also be found in the adrenal medulla (3/3 dogs, Fig. 4C), dorsal root ganglia (1/3 dogs) and myenteric plexus (1/3 dogs), as well as in other areas of the brain. They were very uncommon in the cerebral cortex. Vacuoles were located in neuronal cytoplasm, axon hillocks or rarely in distended axons (Fig. 4B). Most often, 1–2 large, round unstained vacuole or a small cluster of vacuoles were present in neuronal cytoplasm, displacing Nissl substance. Vacuoles did not stain positively with ubiquitin immunohistochemically (not shown) and were negative with oil red O stain (Fig. 4D), which stains neutral triglycerides.

Cerebellar Purkinje cell numbers appeared normal but many of these cells had condensed cytoplasm with central pallor on calbindin staining (Fig. 4B) and a foamy appearance at the light microscopic level in the semi-thin sections of plastic-embedded specimens (Fig. 5A). The nuclei of these cells also appeared condensed (Fig. 5A and C). At the ultrastructural level, the foamy appearance of the perinuclear cytoplasm was found to be due to the presence of numerous small vacuoles (Fig. 5C). At higher magnification, the small vacuoles in the Purkinje cells were mostly clear but some contained clumps of electron dense material (Fig. 5E). Such changes were not seen in similarly processed sections from a control dog (Fig. 5B, D & F).

Electron microscopy revealed that the large vacuoles in the cerebellar roof nuclei were membrane bound and contained scant, fibrillary debris (Fig. 6A and B). Often a mix of small and large vacuoles were found (Fig. 6A and C) and in some cells, large clusters of small vacuoles were present (Fig. 6D). The vacuoles ranged in size from as little as about 0.2 μm up to as much as 20 μm in diameter.

Biopsies were evaluated from the cranial tibial, masseter, triceps, vastus lateralis and left and right cricoarytenoideus dorsalis muscles. Numerous atrophic fibers having an angular to anguloid shape were noted in the left (Fig. 7A) and right cricoarytenoideus dorsalis muscles with variable endomysial fibrosis. Similar changes were not observed in comparable samples from an age matched, normal healthy dog (Fig. 7B). Atrophic fibers were only rarely present in the masseter and limb muscles. Fiber type grouping was not observed. Intramuscular nerve branches in the cricoarytenoideus muscles were variably depleted of myelinated fibers. Rare necrotic fibers were present undergoing phagocytosis. Immunohistochemical staining of muscle from an affected dog for the lysosomal marker LC3 and ubiquitin were similar to control muscle and oil red O staining did not demonstrate excessive lipid accumulation (data not shown). Peripheral nerve specimens were evaluated from the left (Fig. 7C) and right recurrent laryngeal nerves, left and right cranial laryngeal nerves, radial and sciatic nerves. Recurrent laryngeal nerves showed marked nerve fiber loss in the affected dog (Fig. 7C) but not in the normal dog (Fig. 7D).

At the electron microscopic level, dystrophic changes consisting of aggregates of vesicular structures (Fig. 8A) and scattered organelles (Fig. 8B) were seen in axons of the left recurrent laryngeal nerve. An altered myelin periodicity suggested abnormal interactions of axon and myelin at the interglial loop of this nerve (Fig. 8B).

4. Discussion

The BRT disease we studied had been briefly described as a peripheral axonal neuropathy in a review of heritable canine motor and sensory neuropathies (Granger, 2011). Because we have extended the disease description to include not only the polyneuropathy, but also ocular abnormalities and neuronal vacuolation, we now use POANV to refer to the disease. The WGS of a POANV-affected dog contained a homozygous *RAB3GAP1* single nucleotide deletion, *RAB3GAP1*:*c.743delC*. All 13 POANV-affected BRT represented in our DNA collection tested homozygous for this deletion; whereas, none of our other DNA samples from 249 BRT or 100 dogs of other breeds were homozygous for the *c.743delC* allele. The *RAB3GAP1*:*c.743delC* produces a frame shift that predicts a premature stop codon and a truncated gene product *RAB3GAP1*:*p.P248Lfs4** missing 730 C-terminal amino acids, including the catalytic domain. Thus, it is doubtful that the truncated gene product retains biological activity. While this manuscript was in review,

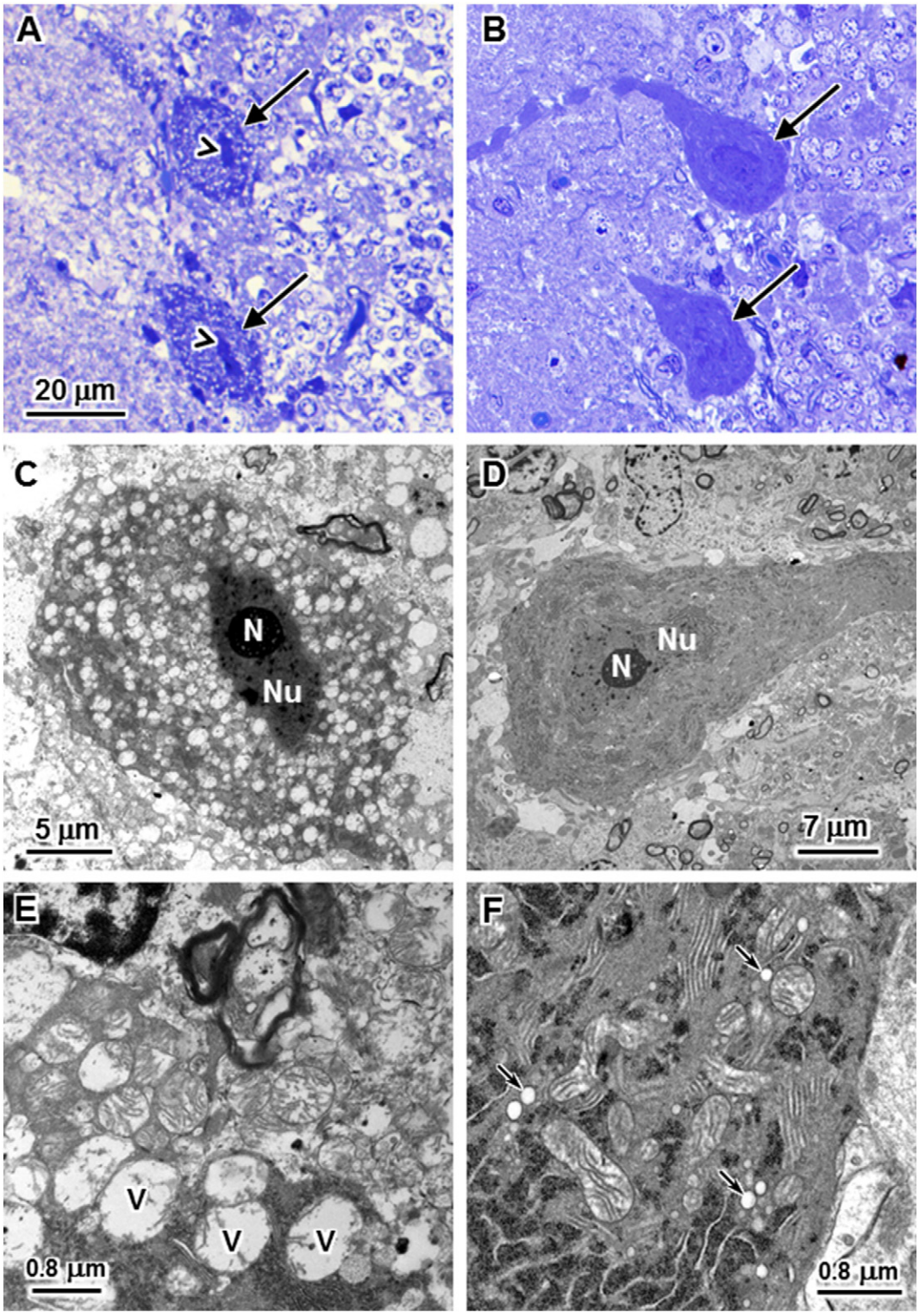

Fig. 5. Numerous, small vacuoles are present in the Purkinje cell bodies of dogs with POANV (A, C, and E) that are not observed in the Purkinje cells of a normal dog (B, D, and F). With light microscopy the Purkinje cell cytoplasm has a foamy appearance (arrows in A) and the cell nuclei are highly condensed (arrowheads in A). In contrast, the Purkinje cell cytoplasm of normal dogs (arrows in B) is more uniformly stained and the nuclei are much less compressed. With electron microscopy (C and E), the foamy appearance of the cytoplasm was observed to be due to the presence of numerous vacuoles throughout the Purkinje cell bodies. Many of these vacuoles were up to 1 µm in diameter (labeled "v" in panel E). With electron microscopy no corresponding vacuoles were observed in the Purkinje cell bodies of a normal dog (D and F). Small clear vesicles typical of normal endosomes were present in Purkinje cells of the normal dog (arrows in F). N: nucleolus; Nu: nucleus. Bar in (A) indicates the magnification of the micrographs in both panels A and B.

researchers at the University of Bern independently identified a SINE insert in *RAB3GAP1* in Alaskan Husky dogs with a similar phenotype (Wiedmer et al., 2015). Affected Huskies presented with identical ocular changes, weakness, and sensory ataxia. Laryngeal paralysis was not reported though voice change and megaesophagus were. Histopathology showed similar axonal peripheral neuropathy and neuronal vacuolation with more prominent changes reported in the spinal cord white matter. The identification of a different variant in *RAB3GAP1* in dogs

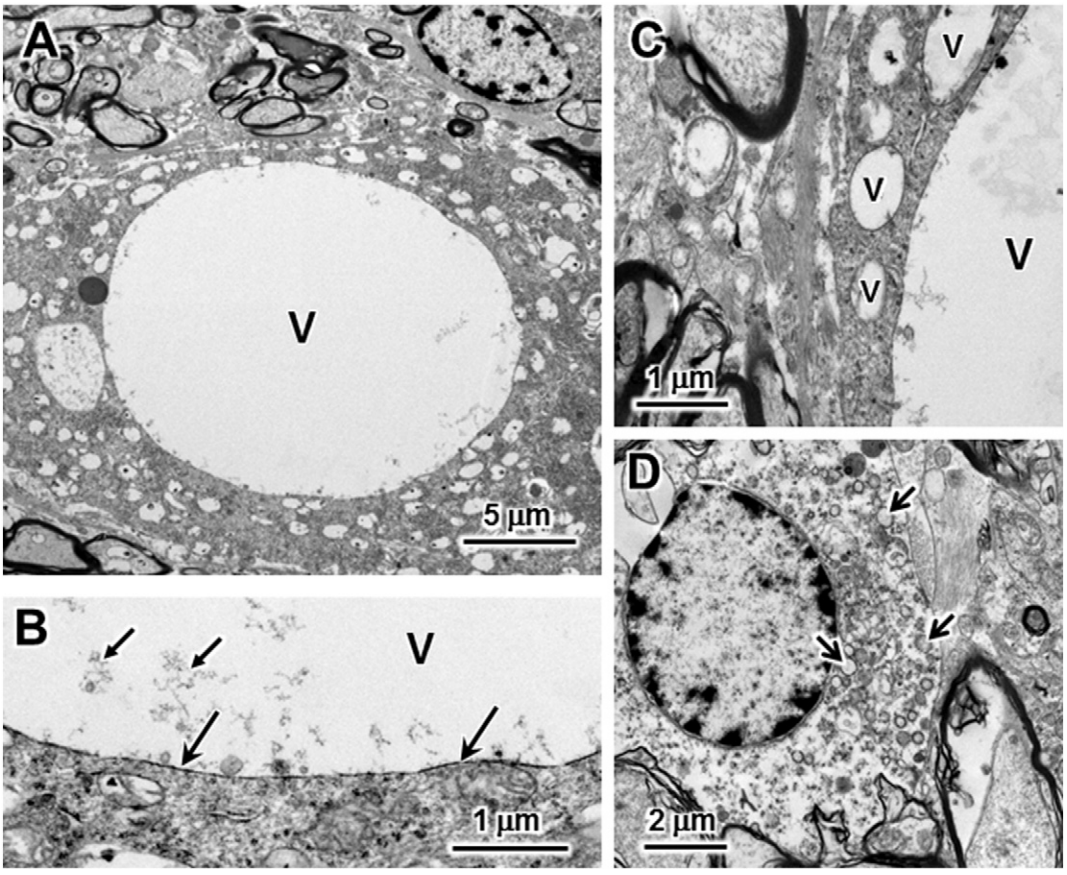

Fig. 6. Large and small vacuoles in neurons of the cerebellar roof nuclei in POANV. (A) Electron micrograph of a large vacuole (V) in a cerebellar roof nucleus neuron. The large vacuoles were mostly clear except for small amounts of loosely aggregated material, primarily near the outer edges of the vacuoles. (B) A higher magnification electron micrograph of the edge of a large vacuole (V) demonstrating that the vacuole was membrane bound (large arrows) and showing some of the aggregated material within the vacuole (small arrows). (C) Vacuoles (V) of intermediate size were often adjacent to the very large vacuoles in some of the cerebellar roof nuclei. (D) Some of the cerebellar roof nuclei neurons had aggregates of numerous small vacuoles (arrows).

with an almost identical phenotype further supports the causality of these variants.

RAB3GAP1 was first recognized and named because it encodes a catalytic subunit that combines with a non-catalytic subunit encoded by *RAB3GAP2*, to form Rab3GAP, a GTPase activator protein (GAP) which greatly enhances the inherent GTPase activity of the four related mammalian Rab3s (Rab3A, -B, -C and -D) (Fukui et al., 1997; Hutagalung and Novick, 2011; Nagano et al., 1998). The Rab3s are members of the Rab family of small GTPases that function as molecular "switches" that regulate the formation, transport, tethering and fusion of a variety of membrane structures by cycling between inactive GDP-bound and active GTP-bound states (Fig. 9) (Bhuin and Roy, 2014; Hutagalung and Novick, 2011).

Homozygous mutations in human *RAB3GAP1* cause either WARBM, characterized by severe developmental deficiencies of the nervous system, eyes and genitalia or Martsolf syndrome with similar but less severe developmental deficiencies. The ocular abnormalities in children with WARBM include congenital cataracts, microphthalmia, microcornea, small atonic pupils and optic nerve atrophy (Handley et al., 2013). Ocular finding in dogs with POANV were similar except that persistent pupillary membranes were also found in two dogs. Neurologic abnormalities in WARBM include microcephaly, seizures, and severe developmental delay with most children never progressing past 4 month stage milestones (Handley et al., 2013). Predominantly frontal polymicrogyria, enlarged sulci, thinning of the corpus callosum and cerebellar hypoplasia were detected in WARBM patients by magnetic resonance imaging (Handley et al., 2013; Morris-Rosendahl et al., 2010). Dogs with POANV exhibit normal behavior and they do not have microcephaly, cortical dysplasias or seizures. No signs of the cerebellar ataxia or cerebellar atrophy reported in WARBM were seen in affected BRT though neurons in the cerebellar roof nuclei and Purkinje cells exhibited histopathological changes.

WARBM patients never develop the ability to crawl or walk. They show hypotonia and evidence of a predominantly axonal peripheral neuropathy (Graham et al., 2004; Nassogne et al., 2000). As in the original report of the condition in BRT (Granger, 2011), affected dogs in this study presented with juvenile onset laryngeal paralysis and polyneuropathy that is predominantly axonal based on the moderate changes in MNCV and predominantly axonal changes on histopathology. These abnormalities are similar to autosomal recessive, axonal, Charcot–Marie–Tooth disease with vocal cord paresis (CMT4A) in humans which has been associated with mutations in an unrelated gene *GDAP1* (Baxter et al., 2002; Cuesta et al., 2002; Sevilla et al., 2003). In WARBM, hypotonia progresses to spastic quadriplegia (Handley et al., 2013). All affected BRT died or were euthanized by 6 months of age, so it is not known whether their weakness would progress from a hypotonic, hyporeflexive to a spastic phenotype.

Nullizygous *Rab3gap1* knockout mice were fertile and no developmental abnormalities were reported in the eyes or the nervous system (Sakane et al., 2006) which highlights the profound differences between knockout models and spontaneous disease. Nonetheless, an increase in Rab3A-bound GTP was detected in brain homogenates from the *Rab3gap1* knockout mice and Ca^{2+}-dependent glutamate release was decreased in synaptosomes isolated from these mice (Sakane et al., 2006). These results were consistent with the Rab3 protein's well established role in exocytosis and neurotransmitter release

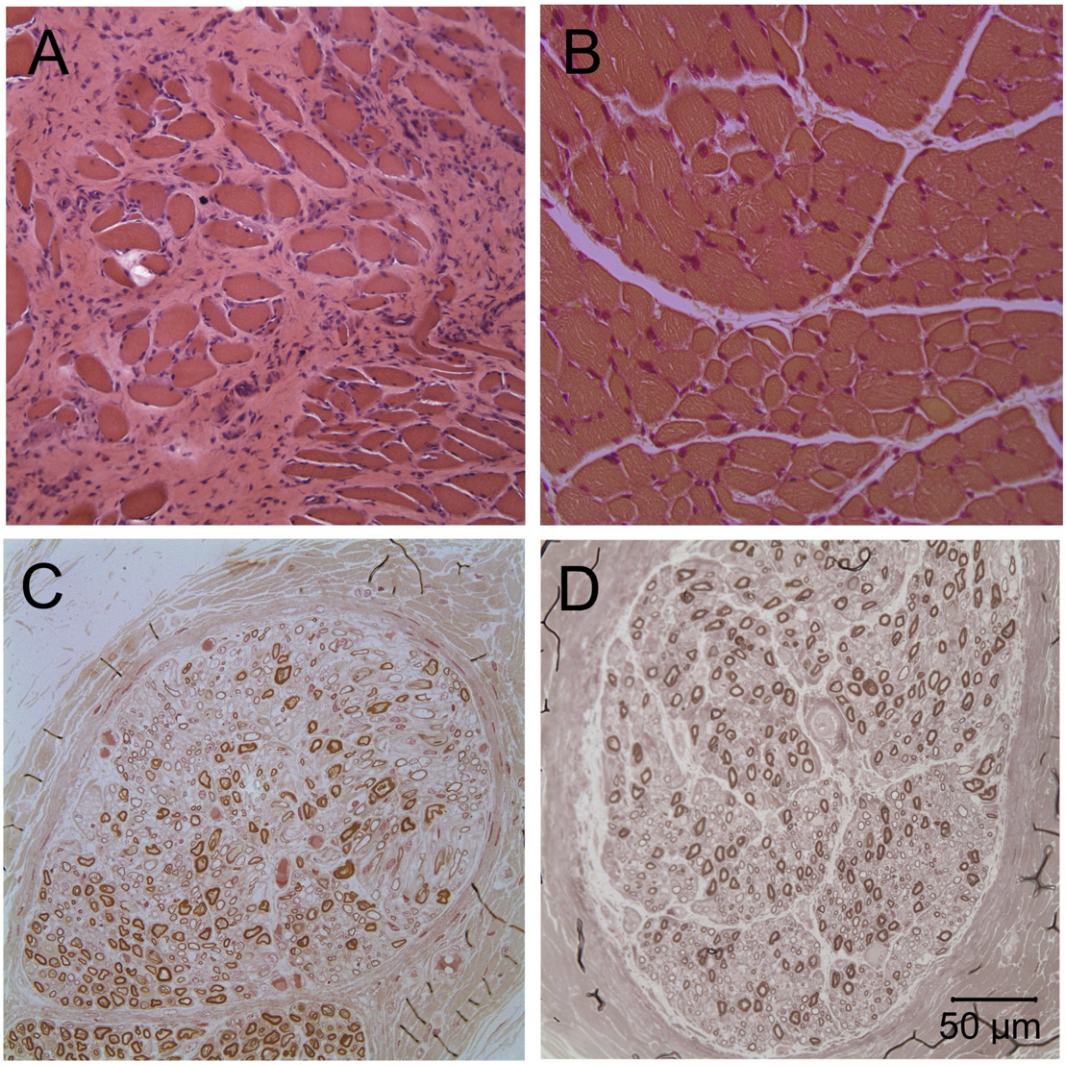

Fig. 7. Cricoarytenoideus muscle from an affected Black Russian Terrier (A) and an age-matched control dog (B). A marked variability in myofiber size with generalized atrophy and endomysial fibrosis is present in the affected dog but not observed in the control dog muscle (H&E stain). A decreased population of large caliber nerve fibers with a subjectively increased population of small caliber fibers was evident in the recurrent laryngeal nerve of the affected Black Russian Terrier dog (C) compared to the age-matched control dog (D) nerve (paraphenylenediamine stain). Bar = 50 μm for all images.

(Hutagalung and Novick, 2011; Muller et al., 2011; Sudhof, 2004), and suggested that altered neurotransmission could be involved in the pathogenesis of WARBM (Aligianis et al., 2005; Aligianis et al., 2006). On the other hand, no mutations in any of the four *RAB3* family genes have been associated with WARBM. In addition, the phenotypes of nullizygous *Rab3* knockout mice do not support a role for *Rab3*-related pathways in the pathogenesis of WARBM. The lack of disease phenotypes in mice with individual *Rab3* gene knockouts has been attributed to redundant functions allowing the remaining *Rab3* genes to compensate for the knocked-out gene. Quadruple knockout mice without any functional Rab3 die from respiratory failure shortly after birth, but unlike WARBM patients these mice have normally developing eyes and brains (Schluter et al., 2004).

WARBM-causing mutations have been reported in three other genes: *RAB3GAP2*, *RAB18* and *TBC1D20* (Aligianis et al., 2006; Bem et al., 2011; Liegel et al., 2013). *TBC1D20* encodes a protein that functions as a GAP for Rab1 and Rab2, which facilitate ER-Golgi trafficking (Liegel et al., 2013). Mice with a spontaneous *Tbc1c20* mutation and *Tbc1d20* knockout mice have congenital cataracts and male sterility (Liegel et al., 2013; Park et al., 2014). *Rab18* knockout mice show cataracts, weakness, and peripheral neuropathy (Bem et al., 2011; Carpanini et al., 2014). The protein encoded by *Rab18* is also involved in ER-golgi trafficking (Dejgaard et al., 2008; Pulido et al., 2011) as well as the assembly of secretory granules (Vazquez-Martinez et al., 2007), and peroxisomes (Gronemeyer et al., 2013). Until recently, it was difficult to understand how mutations in *TBC1D20* and *RAB18* that regulate ER-golgi trafficking could produce disease phenotypes that were indistinguishable from those produced by mutations in the Rab3GAP subunits, originally thought to regulate neurotransmitter release. A plausible explanation was provided by Gerondopoulos et al. who reported that Rab3GAP not only functions as a GAP for the Rab3s but also functions as a guanine exchange factor (GEF) for Rab18. They further showed that Rab3GAP localizes to the ER and that some point mutations in *RAB3GAP1* that cause WARBM in humans affect Rab18 GEF activity but not the GAP activity toward the Rab3 family of proteins (Gerondopoulos et al., 2014). Therefore, the clinical and morphologic abnormalities associated with WARBM and POANV may be related to altered interaction of Rab3GAP1 with Rab18.

Histopathology of the central nervous system from WARBM patients has not been reported. No central nervous system changes were reported in the description of R*ab3gap1* and *Rab18* knockout mice, (Carpanini et al., 2014; Sakane et al., 2006). In BRT with POANV, large vacuoles

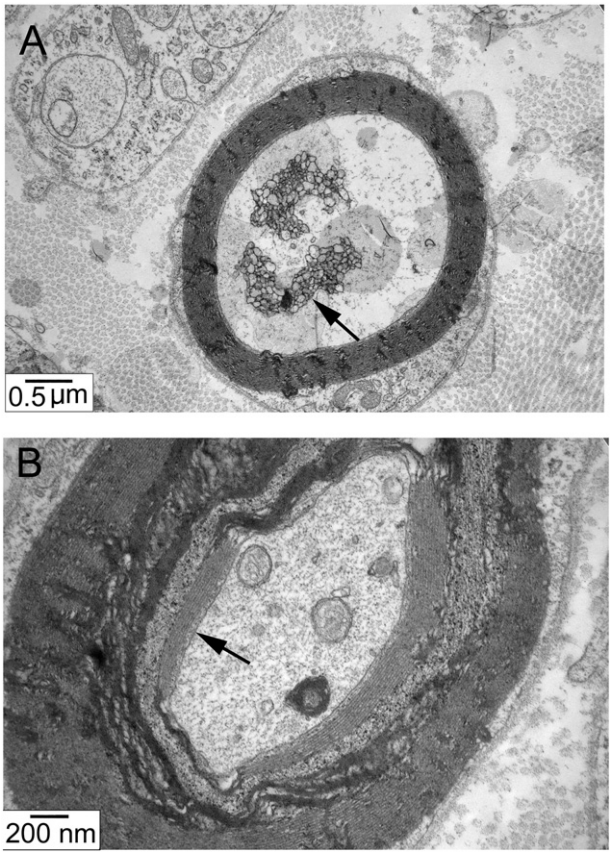

Fig. 8. Electron micrographs from the left recurrent laryngeal nerve of an affected BRT showing clusters of tubular structures resembling abnormally proliferating ER (arrow) (A). Areas of altered myelin periodicity (B, arrow) and abnormal connections between myelin and axons were present at the interglial loop of the left recurrent laryngeal nerve (B).

were visible within neurons of the cerebellar roof nuclei and other areas on light microscopy. On electron microscopy, these cytoplasmic vacuoles appeared as single-membrane bound vacuoles containing scant, fibrous material. In addition to the large, often multiple vacuoles seen on light microscopy, numerous, small and intermediately sized vacuoles were found in the cerebellum, sometimes containing a dense core of material. Small vacuoles or vesicles were also present in axons of the laryngeal nerves and Purkinje cells, either individually, or in clusters.

The formation of intraneuronal vacuoles in POANV could provide clues to the role of Rab proteins in the pathogenesis of WARBM. Rab18 has been shown to be associated with lipid droplet formation in both adipocytes and non-adipocyte cells (Martin et al., 2005; Ozeki et al., 2005). Loss of function of Rab18, Rab3GAP subunits or TBC1D20 increases lipid storage in cells cultured with oleic acid (Gerondopoulos et al., 2014; Liegel et al., 2013; Park et al., 2014). Muscle and cerebellum from affected BRT, however, showed no excessive lipid accumulation on oil red O staining, indicating that the intraneuronal vacuoles were not enlarged lipid droplets. Recent studies have also shown that Rab3GAP subunits regulate autophagy in *Drosophila* and *Caenorhabditis elegans* muscle as well as human fibroblast cultures by affecting autophagosome maturation independent of Rab3 (Spang et al., 2014; Zirin et al., 2015). Intraneuronal vacuoles were recently reported in a spontaneous neurodegenerative disease in Lagotto Romagnolo dogs associated with a mutation in the autophagy-related gene *ATG4D* (Kyostila et al., 2015). In these studies, abnormal autophagosome maturation was demonstrated with LC3 immunohistochemistry (Kyostila et al., 2015; Spang et al., 2014; Zirin et al., 2015). The vacuoles found in affected Lagotto Romagnolo dogs sometimes contained membranous profiles or floccular material typical of a lysosomal storage disease, and axonal swellings contained double-membrane bound autophagosomes (Kyostila et al., 2015). None of these indications of autophagosome dysfunction were identified in POANV.

As mentioned earlier, Rab3GAP localizes to the ER. It is necessary for the ER targeting of Rab18. Absence of either Rab3GAP or Rab18 in fibroblast cell culture results in the disruption of ER tubular networks and the abnormal peripheral distribution of ER sheets (Gerondopoulos et al., 2014). The intra-neuronal vacuoles that we detected in the BRT with POANV may be microscopic and ultrastructural manifestations of ER that has been aberrantly distributed due to the absence of Rab3GAP activity.

The most prominent clinical feature of the POANV phenotype is the juvenile onset laryngeal paralysis and polyneuropathy with electrophysiology and nerve pathology suggesting an axonal neuropathy. A predominantly sensory neuropathy in humans (CMT2B) has been associated with variants in the gene for the Rab protein Rab7, which is important for endosomal trafficking, signaling of neurotrophins, and for retrograde axonal transport (Bucci et al., 2012; Bucci and De Luca, 2012; Verhoeven et al., 2003). *Rab18* knockout mice also develop a peripheral neuropathy and weakness (Carpanini et al., 2014). Muscle fiber atrophy was not reported in mice and it was rarely observed in limb muscles of affected BRTs. However, muscle fiber atrophy was evident in both the left and right cricopharyngeal muscles of BRTs. The pattern of fiber atrophy and electrodiagnostic findings are suggestive of denervation, but quantification of motor endplates to prove denervation were not performed. Clinical signs and pathologic changes of a more generalized peripheral neuropathy could have developed if the dogs had survived longer. Dystrophic changes in axons of the sciatic nerve were reported in *Rab18* knockout mice with disorganization of neurofilaments and collections of microtubules predominantly at the neuromuscular junctions (Carpanini et al., 2014). Dystrophic changes in nerves are characterized by accumulations of normal or abnormal appearing organelles and, vacuoles and clusters of tubular rings arising from altered axoplasmic flow (Lampert, 1967). In POANV, more dramatic dystrophic changes were found in the laryngeal nerves with collections of vacuoles, abnormal appearing organelles and clusters of vesicular structures resembling proliferating ER. Finding such changes remote from the cell body suggest that axonal transport of membranes and or vesicles is also disrupted by the *RAB3GAP1* mutation.

In conclusion, BRT with POANV due to a homozygous *RAB3GAP1:c.743delC* mutation share many signs with WARBM patients (Handley et al., 2013; Nassogne et al., 2000) while *Rab3gap1* null mice exhibit only subtle biochemical changes which may not be relevant to WARBM pathogenesis (Sakane et al., 2006). POANV-affected dogs show a progressive polyneuropathy similar to that seen with *Rab18* knockout mice (Carpanini et al., 2014). In addition, these dogs develop a spongiform encephalopathy with interneuronal vacuolation not seen in mouse models of WARBM. Further studies are needed to determine if these vacuoles represent altered intracellular membrane trafficking. The *RAB3GAP1:c.743delC* dogs could serve as a model for investigating the role of Rab3GAP in membrane trafficking and the pathogenesis of diseases such as WARBM.

Acknowledgments

The authors wish to thank all the veterinarians, breeders, and dog owners who assisted in collecting DNA samples and the clinical data, and to thank the Black Russian Terrier Club of America for their financial support. We thank Robert Wayne of the University of California Los Angeles, Matt Huntelman of the Translational Genomics Research Institute, Kate Meurs and Josh Stern of North Carolina State University and Paula Henthorn of the University of Pennsylvania for providing genome sequence data for use as controls. We thank Dr. Ulrich Koch for the cataract photographs and Cheryl Jensen and Jesus Macias for technical assistance.

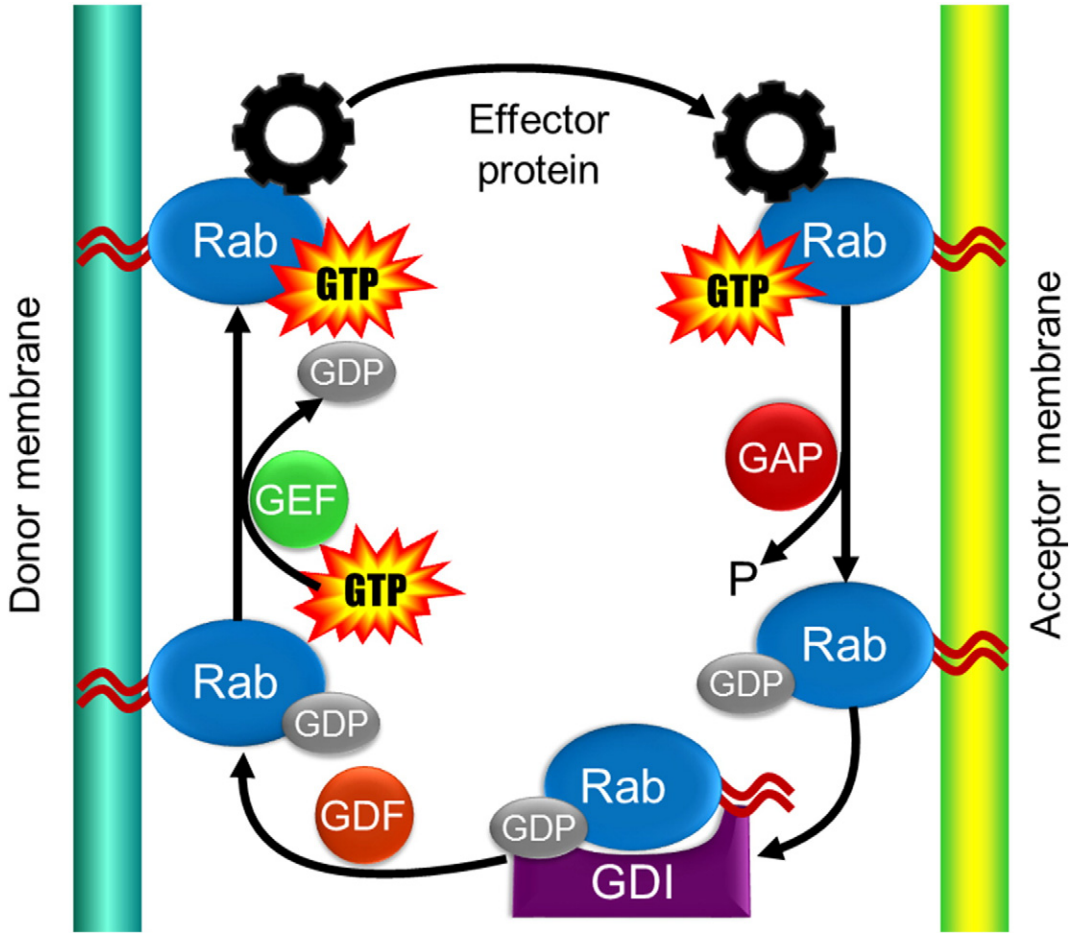

Fig. 9. Membrane bound Rab proteins are activated when a guanine nucleotide exchange factor (GEF) exchanges GDP with GTP. They act through an effector molecule to form, transport, tether or fuse to an acceptor membrane. An associated GTPase activator protein (GAP) greatly enhances the inherent GTPase activities of the Rab to hydrolyze GTP to GDP inactivating the Rab. The Rab is then removed from the acceptor membrane by the guanine nucleotide dissociation inhibitor (GDI). The GDI dissociation factor (GDF) returns the Rab protein to the donor membrane in preparation for the next cycle (Bhuin and Roy, 2014; Hutagalung and Novick, 2011). Rab3Gap1/2 functions as both a GAP for Rab3 and a GEF for Rab18 (Fukui et al., 1997; Gerondopoulos et al., 2014; Hutagalung and Novick, 2011; Nagano et al., 1998). Disruption of this process in POANV may explain the membrane trafficking abnormalities found on histopathology.

Appendix A. Supplementary data

Supplementary data to this article can be found online at http://dx.doi.org/10.1016/j.nbd.2015.11.016.

References

Aligianis, I.A., et al., 2005. Mutations of the catalytic subunit of RAB3GAP cause Warburg micro syndrome. Nat. Genet. 37, 221–223.

Aligianis, I.A., et al., 2006. Mutation in Rab3 GTPase-activating protein (RAB3GAP) noncatalytic subunit in a kindred with Martsolf syndrome. Am. J. Hum. Genet. 78, 702–707.

Bancroft, J.D., Gamble, M., 2008. Theory and Practice of Histological Techniques. Churchill Livingstone Elsevier, North Hollywood, CA.

Baxter, R.V., et al., 2002. Ganglioside-induced differentiation-associated protein-1 is mutant in Charcot–Marie–Tooth disease type 4A/8q21. Nat. Genet. 30, 21–22.

Beggs, A.H., et al., 2010. MTM1 mutation associated with X-linked myotubular myopathy in Labrador retrievers. Proc. Natl. Acad. Sci. U. S. A. 107, 14697–14702.

Bem, D., et al., 2011. Loss-of-function mutations in RAB18 cause Warburg micro syndrome. Am. J. Hum. Genet. 88, 499–507.

Bhuin, T., Roy, J.K., 2014. Rab proteins: the key regulators of intracellular vesicle transport. Exp. Cell Res. 328, 1–19.

Bucci, C., et al., 2012. Charcot–Marie–Tooth disease and intracellular traffic. Prog. Neurobiol. 99, 191–225.

Bucci, C., De Luca, M., 2012. Molecular basis of Charcot–Marie–Tooth type 2B disease. Biochem. Soc. Trans. 40, 1368–1372.

Carpanini, S.M., et al., 2014. A novel mouse model of Warburg micro syndrome reveals roles for RAB18 in eye development and organisation of the neuronal cytoskeleton. Dis. Model Mech. 7, 711–722.

Cuesta, A., et al., 2002. The gene encoding ganglioside-induced differentiation-associated protein 1 is mutated in axonal Charcot–Marie–Tooth type 4A disease. Nat. Genet. 30, 22–25.

Dejgaard, S.Y., et al., 2008. Rab18 and Rab43 have key roles in ER-Golgi trafficking. J. Cell Sci. 121, 2768–2781.

Dubowitz, V., Sewry, C.A., 2013. Histological and histochemical stains and reactions. In: Dubowitz, V., et al. (Eds.), Muscle Biopsy: A Practical Approach. Saunders Elsevier, St. Louis, pp. 16–27.

Fischer von Mollard, G., et al., 1990. rab3 is a small GTP-binding protein exclusively localized to synaptic vesicles. Proc. Natl. Acad. Sci. U. S. A. 87, 1988–1992.

Fukui, K., et al., 1997. Isolation and characterization of a GTPase activating protein specific for the Rab3 subfamily of small G proteins. J. Biol. Chem. 272, 4655–4658.

Gerondopoulos, A., et al., 2014. Rab18 and a Rab18 GEF complex are required for normal ER structure. J. Cell Biol. 205, 707–720.

Graham Jr., J.M., et al., 2004. MICRO syndrome: an entity distinct from COFS syndrome. Am. J. Med. Genet. A 128a, 235–245.

Granger, N., 2011. Canine inherited motor and sensory neuropathies: an updated classification in 22 breeds and comparison to Charcot–Marie–Tooth disease. Vet. J. 188, 274–285.

Gronemeyer, T., et al., 2013. Localization of Rab proteins to peroxisomes: a proteomics and immunofluorescence study. FEBS Lett. 587, 328–338.

Handley, M.T., et al., 2013. Mutation spectrum in RAB3GAP1, RAB3GAP2, and RAB18 and genotype-phenotype correlations in Warburg micro syndrome and Martsolf syndrome. Hum. Mutat. 34, 686–696.

Henkel, C.K., et al., 2005. Quantitative assessment of developing afferent patterns in the cat inferior colliculus revealed with calbindin immunohistochemistry and tract tracing methods. Neuroscience 136, 945–955.

Hutagalung, A.H., Novick, P.J., 2011. Role of Rab GTPases in membrane traffic and cell physiology. Physiol. Rev. 91, 119–149.

Katz, M.L., et al., 2005. A mutation in the CLN8 gene in English setter dogs with neuronal ceroid-lipofuscinosis. Biochem. Biophys. Res. Commun. 327, 541–547.

Kyostila, K., et al., 2015. A missense change in the ATG4D gene links aberrant autophagy to a neurodegenerative vacuolar storage disease. PLoS Genet. 11, e1005169.
Lampert, P.W., 1967. A comparative electron microscopic study of reactive, degenerating, regenerating, and dystrophic axons. J. Neuropathol. Exp. Neurol. 26, 345–368.
Liegel, R.P., et al., 2013. Loss-of-function mutations in TBC1D20 cause cataracts and male infertility in blind sterile mice and Warburg micro syndrome in humans. Am. J. Hum. Genet. 93, 1001–1014.
Livak, K.J., 1999. Allelic discrimination using fluorogenic probes and the 5′ nuclease assay. Genet. Anal. 14, 143–149.
Martin, S., et al., 2005. Regulated localization of Rab18 to lipid droplets: effects of lipolytic stimulation and inhibition of lipid droplet catabolism. J. Biol. Chem. 280, 42325–42335.
Morris-Rosendahl, D.J., et al., 2010. New RAB3GAP1 mutations in patients with Warburg micro syndrome from different ethnic backgrounds and a possible founder effect in the Danish. Eur. J. Hum. Genet. 18, 1100–1106.
Muller, M., et al., 2011. Rab3-GAP controls the progression of synaptic homeostasis at a late stage of vesicle release. Neuron 69, 749–762.
Nagano, F., et al., 1998. Molecular cloning and characterization of the noncatalytic subunit of the Rab3 subfamily-specific GTPase-activating protein. J. Biol. Chem. 273, 24781–24785.
Nassogne, M.C., et al., 2000. Polymicrogyria and motor neuropathy in micro syndrome. Neuropediatrics 31, 218–221.
Ozeki, S., et al., 2005. Rab18 localizes to lipid droplets and induces their close apposition to the endoplasmic reticulum-derived membrane. J. Cell Sci. 118, 2601–2611.
Park, A., et al., 2014. Targeted disruption of Tbc1d20 with zinc-finger nucleases causes cataracts and testicular abnormalities in mice. BMC Genet. 15, 135.
Pulido, M.R., et al., 2011. Rab18 dynamics in adipocytes in relation to lipogenesis, lipolysis and obesity. PLoS ONE 6, e22931.
Rossor, A.M., et al., 2013. Clinical implications of genetic advances in Charcot–Marie–Tooth disease. Nat. Rev. Neurol. 9, 562–571.
Sakane, A., et al., 2006. Rab3 GTPase-activating protein regulates synaptic transmission and plasticity through the inactivation of Rab3. Proc. Natl. Acad. Sci. U. S. A. 103, 10029–10034.
Schluter, O.M., et al., 2004. A complete genetic analysis of neuronal Rab3 function. J. Neurosci. 24, 6629–6637.
Sevilla, T., et al., 2003. Clinical, electrophysiological and morphological findings of Charcot–Marie–Tooth neuropathy with vocal cord palsy and mutations in the GDAP1 gene. Brain 126, 2023–2033.
Sheehan, D.C., Hrapchak, B.R., 1980. Theory and Practice of Histotechnology. CV Mosby, St. Louis.
Sims, M.H., Redding, R.W., 1980. Maturation of nerve conduction velocity and the evoked muscle potential in the dog. Am. J. Vet. Res. 41, 1247–1252.
Spang, N., et al., 2014. RAB3GAP1 and RAB3GAP2 modulate basal and rapamycin-induced autophagy. Autophagy 10, 2297–2309.
Sudhof, T.C., 2004. The synaptic vesicle cycle. Annu. Rev. Neurosci. 27, 509–547.
Swallow, J.S., Griffiths, I.R., 1977. Age related changes in the motor nerve conduction velocity in dogs. Res. Vet. Sci. 23, 29–32.
Vallat, J.M., et al., 2013. The various Charcot–Marie–Tooth diseases. Curr. Opin. Neurol. 26, 473–480.
Vazquez-Martinez, R., et al., 2007. Rab18 inhibits secretory activity in neuroendocrine cells by interacting with secretory granules. Traffic 8, 867–882.
Verhoeven, K., et al., 2003. Mutations in the small GTP-ase late endosomal protein RAB7 cause Charcot–Marie–Tooth type 2B neuropathy. Am. J. Hum. Genet. 72, 722–727.
Walker, T.J., et al., 1979. Motor nerve conduction velocity and latency in the dog. Amer. J. Vet. Res. 40, 1433–1439.
Warburg, M., et al., 1993. Autosomal recessive microcephaly, microcornea, congenital cataract, mental retardation, optic atrophy, and hypogenitalism. Micro syndrome. Am J Dis Child. 147, 1309–1312.
Wiedmer, M., Oevermann, A., Borer-Germann, S.E., Gorgas, D., Shelton, G.D., Jagannathan, V., Henke, D., Leeb, T., 2015. A RAB3GAP1 SINE insertion in Alaskan Huskies with polyneuropathy, ocular abnormalities and neuronal vacuolation (POANV) resembling human Warburg Micro Syndrome 1 (WARBM1). http://dx.doi.org/10.1534/g3.115.022707 (g3.115.022707; Early Online November 23, 2015).
Zeng, R., et al., 2014. Breed distribution of SOD1 alleles previously associated with canine degenerative myelopathy. J. Vet. Intern. Med. 28, 515–521.
Zimin, A.V., et al., 2013. The MaSuRCA genome assembler. Bioinformatics 29, 2669–2677.
Zirin, J., et al., 2015. Regulators of autophagosome formation in drosophila muscles. PLoS Genet. 11, e1005006.